JOURNAL OF MECHANICAL ENGINEERING AND SCIENCES
ISSN: 2289-4659 e-ISSN: 2231-8380
VOLUME 20, ISSUE 2, 2026, 11194 - 11208
DOI: https://doi.org/10.15282/jmes.20.2.2026.5.0873

RESEARCH ARTICLE

Experimental study on the propagation characteristics of the rotating detonation wave of a small-scale rotating detonation engine

Mohd Fahmi Md Salleh[1,2]*, Mazlan Abdul Wahid[1]*, Hussein A. Mohammed[3]*, Natrah Kamaruzaman[1], Umar Ikhwan Mohd Rozaiddin[4], Ahmad Dairobi Ghazali[1]

[1]High Speed Reacting Flow Laboratory, Faculty of Mechanical Engineering, Universiti Teknologi Malaysia, 81310 Skudai, Johor, Malaysia
[2]Faculty of Mechanical Engineering, Universiti Teknologi MARA, Johor Branch, Pasir Gudang Campus, 81750 Masai, Johor, Malaysia, Phone: +6073818470
[3]Mechanical Engineering Department, King Fahd University of Petroleum & Minerals, Dhahran 31261, Saudi Arabia
[4]West Virginia University, Morgantown, West Virginia 26506-6106, United States of America

Abstract - Detonation combustion modes offer potential benefit over deflagration-based combustion due to rapid heat release and pressure-gain characteristics. A small-scale rotating detonation engine (RDE) is a compact detonation-based device capable of continuous and high-frequency operation. Small-scale RDEs are promising for propulsion related and laboratory-scale applications, especially for compact operation under low flow-rate conditions. In the present study, wave propagation behaviour in a small-scale RDE running on methane–oxygen was investigated experimentally using high-speed imaging. The combustor annulus had an inner diameter and outer diameter of 38 mm and 46 mm, respectively. The operating conditions were varied over equivalence ratios (φ = 0.8–1.2) and total mass flow rates ($\dot{m}$total = 3.8, 4.0, and 4.2 g/s). The high-speed image sequences showed alternating single-wave and dual-wave propagation modes within the RDE annulus under the tested conditions. The wave propagation velocity and wave propagation frequency were determined from the recorded image sequences. The average wave propagation velocity was found to be significantly lower than the ideal Chapman–Jouguet value, indicating non-ideal wave behaviour under the present low flow rate operating conditions. Overall, the results provide useful insight into the propagation characteristics of a small-scale RDE operating with methane–oxygen mixtures at very low total mass flow rates.

Article History
Received : 24 November 2025
Revised : 16 February 2026
Accepted : 9 June 2026
Published : 30 June 2026

Keywords
Rotating detonation engine
Combustor
Equivalence ratio
Total mass flow rates
High-speed images

1. Introduction

Detonation-based engines, such as pulse detonation engines and rotating detonation engines (RDEs), have the potential to be used in propulsion and power generation systems. Unlike conventional combustion systems that operate via deflagration, detonation-based engines operate via supersonic combustion processes, in which the shock wave and the exothermic reaction zone are tightly coupled [1]. This coupling leads to pressure-gain combustion, in which pressure and temperature increase abruptly while the specific volume decreases slightly as the detonation front propagates through the reactants [2]. Compared with deflagration-based combustion processes, detonation-based combustion enables faster energy release with lower entropy generation, potentially resulting in higher thermodynamic efficiency [1]. Among the detonation-based engines, the RDE has been considered as a promising candidate for practical implementation. Unlike the PDE, which requires cyclic filling, ignition, and purging processes, the RDE operates via a single initiation to generate continuous, propagating detonation waves within an annular combustion chamber, enabling near-uniform thrust generation [3]. Previous studies have reported that the detonation wave propagation frequency in RDE typically lies within the range of 1–100 kHz depending on the fuel composition, equivalence ratio and combustor geometry [3], [4]. The operating frequency of the RDE is significantly higher than that of the PDE, which generally operates below 100 Hz [5]. Furthermore, the high operating frequency of RDE enables continuous engine operation, potentially improving propulsion performance and combustion stability [6]. In addition, thermodynamic analysis suggests that RDE may achieve approximately 20% higher efficiency than conventional Brayton-cycle devices [7]. Therefore, RDEs offer greater potential for implementation in propulsion technologies and for further improving the power generation cycle.

An RDE configuration consists of two coaxial cylinders that form an annular combustion chamber [8]. The reactants are continuously supplied through the injector ports of the RDE to several micro-nozzles or slits, located upstream of the annular combustion chamber. Compared with liquid fuels, gaseous fuel injection generally provides faster mixing and simpler injection systems, making it a primary choice for RDE experiments [9]. Once the reactant mixture is ignited, one or more rotating detonation waves propagate circumferentially within the annular combustion chamber. The detonation wave compresses the incoming fresh reactant mixture and sustains the combustion as long as the reactants are continuously supplied. The high-pressure combustion products subsequently expand and flow toward the downstream end of the RDE combustor, exiting primarily in the axial direction and generating thrust [1]. Additionally, the downstream end of the RDE can be integrated with nozzles to accommodate specific application needs and provide design flexibility [10]-[11]. In recent years, the development of small-scale RDE has caught the attention of the RDE research community. Small-scale configurations of the RDE offer several advantages, including reduced material usage, compact design and

*CORRESPONDING AUTHOR | Mohd Fahmi Md Salleh | ✉ fahmisalleh@uitm.edu.my

improved suitability for limited testing facilities, such as laboratory-scale investigations [12]-[14]. Furthermore, small-scale RDE investigations provide valuable insights into the fundamental characteristics of detonation wave behaviour and may be used to inform future upscaling and practical implementation [12]. Compared with larger RDE configurations, small-scale RDEs typically feature shorter annular channels, which reduce the propagation distance of the detonation wave. These conditions lead to shorter refill intervals and reactant mixture refreshment times during RDE operation [11]. As a result, the stability of the detonation wave can be significantly influenced by incomplete reactant mixing, injector configuration, and pressure feedback within the RDE combustion chamber [15]. In addition, premature deflagration, weaker detonation waves, and slower heat release may cause the detonation wave to fail to sustain due to insufficient reactant mixing [16]. These challenges become particularly significant when the small-scale RDE is operated at low total mass flow rates, where the reduced reactant momentum and weaker mixing characteristics may affect the formation of a stable detonation wave.

Previous studies have investigated small-scale RDEs employing various fuel and oxidiser combinations, including ethylene-oxygen [10], hydrogen-oxygen [12], and methane-oxygen mixtures [17]–[19]. Among these combinations, methane-oxygen has been widely adopted due to its relatively well-characterised detonation properties and suitability for laboratory experiments. A survey of the literature indicates that most small-scale RDE studies are conducted at total mass flow rates ranging approximately from 0.05 kg/s to 0.375 kg/s [10], [14], [20]. These studies have contributed significantly to the understanding of detonation wave behaviour, including the formation of single- and multiple-rotating detonation waves and the influence of injector design and combustor geometry on engine performance [21]-[22]. In some cases, transitions between different detonation modes have also been observed, which may lead to instabilities such as mode switching [23]. Despite the progress reported in the previous studies, investigations on small-scale RDE operation at very low total mass flow rates remain limited. Only a small number of studies have explored the small-scale RDE operation in the gram-per-second regime. For example, Keller et al. [24] and Law et al. [11] have investigated ethylene-oxygen mixtures at total mass flow rates between approximately 0.0035–0.0097 kg/s. Operating a small-scale RDE at such minimal flow rates may contribute towards more compact propulsion devices and laboratory-scale experimental platforms. However, the characteristics of detonation wave propagation under these low-flow-rate conditions remain poorly understood, particularly for methane-oxygen mixtures in small-scale annular RDEs. Although RDE operation appears conceptually straightforward, its successful performance is strongly influenced by the interaction of chemical processes, combustor geometry and flow operating conditions, particularly in small-scale configurations [14].

The propagation velocity of rotating detonation waves is strongly influenced by the thermochemical reactivity of the supplied reactant mixture and the refill rate of fresh reactants in the annulus [25]-[26]. Generally, an increase in oxygen content enhances the mixture reactivity and sensitivity, promoting faster and more stable wave propagation [27]. Meanwhile, higher reactant temperatures accelerate the reaction rates and reduce ignition delays [28]. In addition, the total mass flow rate significantly influences the refill process, mixture availability and uniformity, and pressure recovery ahead of the detonation wave front, especially when the channel length is limited, as in small-scale RDEs [18], [29]. However, the oxygen composition and reactant temperature were not varied independently in the present study. Accordingly, the present investigation focuses on the effects of equivalence ratio and total mass flow rate on wave propagation behaviour. The detonation behaviour of the present small-scale RDE configuration has been previously investigated using high-frequency pressure diagnostics [30]. Based on that earlier work, the present study experimentally visualises wave propagation in a small-scale RDE operating at low total mass flow rates using methane-oxygen mixtures. The study focuses on wave propagation dynamics, including the wave propagation velocity and frequency obtained from high-speed imaging measurements. Two independent operating parameters, the equivalence ratio and the total mass flow rate of the reactant mixture, are systematically varied to examine their influence on wave propagation behaviour. The findings of this study aim to provide a better understanding of wave propagation behaviour in small-scale RDE systems operating at low total mass flow rates, which may contribute to the development of compact detonation-based propulsion and power-generation devices.

2. Materials and Methods

2.1 Small-Scale RDE Test Model Description

The study was conducted using a conventional annular geometry for the RDE combustion chamber characterized by a cylindrical annular channel where the detonation wave propagates circumferentially. The annular geometry has been commonly investigated in previous RDE studies due to its simplicity and effectiveness in sustaining detonation wave propagation [31]. Modular concepts have been employed in the development of the present small-scale RDE test model to ease the fabrication, installation and future modification. There are seven separate modules for the small-scale RDE test model construction as shown in Figure 1 and the general dimensions for the small-scale RDE test model are presented in Table 1. Mild steel was selected for fabricating the small-scale RDE test model in the present study not only due to cost considerations, but also because of its ease of fabrication and suitability for short duration hot tests. Note that the present experiment was conducted for a maximum operating period of approximately 1s, and the material chosen was considered acceptable for this investigation.

The small-scale RDE test model used in the present study was designed based on the recommendations of Bykovskii et al. [21], Dechert et al. [14], and Han et al. [10]. According to Bykovskii et al. [21], the channel width should be at least as large as the detonation cell size. Additionally, there are limitations on the detonation channel length (l_d), channel gap (Δ), and reactant fill height (h) that must be considered to achieve stable RDE operation. In this study, the cell width for the methane-oxygen mixture as described by Malik et al. [32], which ranges from 2.9 mm to 8.3 mm, has been taken into

consideration. Based on the recommendations, the estimated fill height of the reactant mixture was approximately 20.3 mm above the injection surface. The combustor channel length ($L_{combustor}$) chosen and the total small-scale RDE model length (L_{total}) is 50 mm and 100 mm, respectively. The detonation channel width used in the present study is 4 mm, with the inner diameter (D_i) and outer diameter (D_o) of the RDE combustion chamber annulus being 38 mm and 46 mm, respectively. The arrangement of the outer body and centre body, which have a length of 50 mm each, formed the RDE combustor annulus. There is no nozzle, such as an aerospike nozzle, attached to the small-scale RDE in the present study for better visualisation, as suggested by set al. [12].

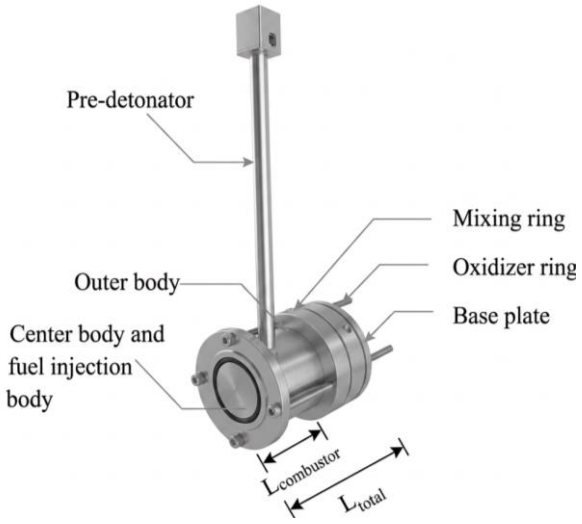

Figure 1. Modular small-scale RDE

Table 1. Geometrical specifications of the small-scale RDE test model

Item	Dimension / specification
Annulus inner diameter	38 mm
Annulus outer diameter	46 mm
Combustor length	50 mm
Outer body length	50 mm
Center body length	50 mm
Mixing area	1 mm gap round slot
Fuel injection body	Ø 0.7 mm × 80 fuel injection holes
Total RDE Length	100 mm

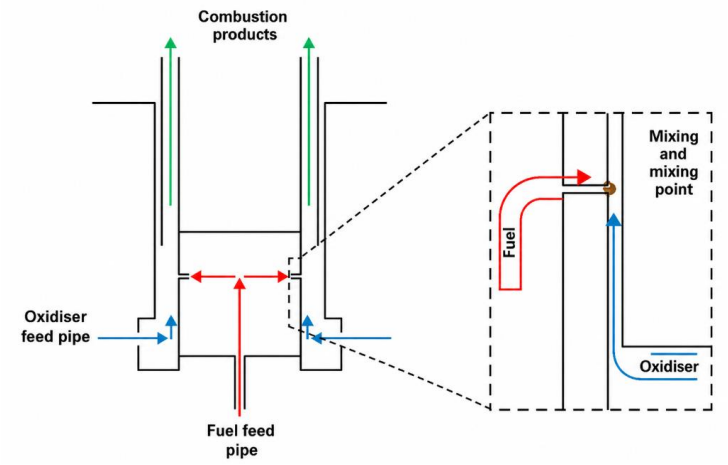

Figure 2. RDE fuel and oxidiser feeding

Figure 2 shows the flow of the fuel and oxidiser fed to the small-scale RDE combustion chamber. The fuel was fed from the base of the RDE and entered the mixing area through 80 injection holes with 0.7 mm diameter to improve the mixture homogeneity [13]. Meanwhile, the oxidiser was fed to the small-scale RDE through four injection ports tangentially located at the oxidiser ring, as shown in Figure 1. Then, the oxidiser flows through the 1mm channel and mixes with the fuel at the mixing point before it enters the RDE annulus, as shown in Figure 2. The mixing strategy used in the present study was based on Rahman [33]. Axial and radial entrances of the fuel and oxidiser were said to have the

potential to facilitate effective mixing of the reactants. This is due to lower maximum mass-fraction values, which are attributed to direct collision between the fuel stream upon entry into the chamber and the oxidiser stream.

2.2 Pre-Detonator

A pre-detonator was used to initiate the detonation wave in this study due to its superior success rate, capability, and repeatability in RDE initiations [6], [34]. The pre-detonator was positioned tangentially 13 mm upstream of the RDE open-end exhaust. Positioning farther from the fuel and oxidiser injectors was suggested by Mazlan et al. [35] to improve mixing as the reactants progress along the RDE combustion chamber. This could lead to a successful initiation and transition to a steady detonation operation. The overall dimensions and diagram of the pre-detonator used in the present study are shown in Figure 3. The pre-detonator has a length of 220mm, divided into a 30mm section to accommodate the spark plug and a 190mm long-tube section. The spark plug was mounted at the top of the pre-detonator to serve as the ignition source. The inner diameter of the pre-detonator was the same as the small-scale RDE channel width, which is 4mm. In this study, a 160 mm-long Shchelkin spiral, a device used to promote deflagration-to-detonation transition (DDT) in the RDE combustion chamber, was placed inside the pre-detonator. Note that a longer Shchelkin spiral increases the resistance within the pre-detonator, intensifying reflections and collisions of the shock front as it interacts with the flame front, thereby increasing DDT intensity and detonation velocity [36].

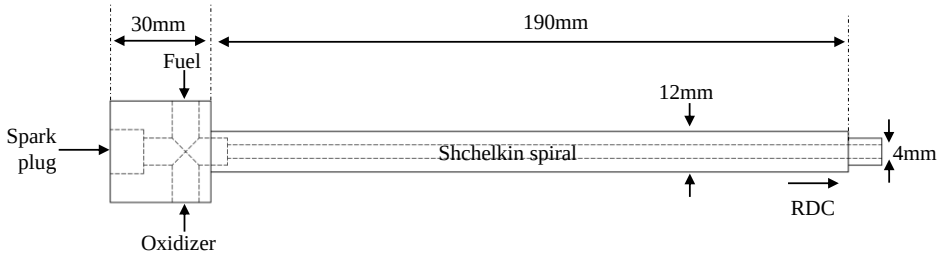

Figure 3. Pre-detonator

2.3 Methodology

2.3.1 RDE experimental facility

The experiments were conducted at High-Speed Reacting Flow Laboratory (HiREF), Universiti Teknologi Malaysia (UTM). There are three rooms utilised to accommodate different functions of the RDE experimental setup, namely the test chamber, operation control room, and gas storage area. The RDE experimental rig was set up on a test bed located in the test chamber. The test chamber has been specifically designed and constructed for safety purposes [13]. This includes the ventilation system for exhausting combustion products and excess fuel gases from the experiments. Meanwhile, the control panel and data acquisition (DAQ) system workstation are in the operation control room. The control panel and DAQ workstation operate the RDE remotely and retrieve experimental data, respectively. This safety protocol is implemented to ensure operator safety during RDE operation. The nature of RDE operation, which involves extremely loud noise, complex detonation waves, pressure fluctuations, and high temperatures, may create potentially hazardous conditions. Furthermore, the exhaust gases produced could be harmful and pose additional risks during the operation. Therefore, strict safety measures and appropriate distance from the engine are essential to protect operating personnel. On the other hand, fuel and oxidisers are stored in the gas storage area outside the HiREF laboratory for safety and regulatory requirements. Safety precautions are required when handling, using and storing, especially the flammable gases [37]. Note that most types of cylinders tend to explode when exposed to intense heat, causing risk to personnel in the vicinity. Thus, the gas cylinders should be stored in a secure, cool, dry place, away from sources of ignition and heat. It is preferable for the storage to be in the open air, but adequate ventilation will be needed to disperse any vapour from the leaking containers. The fuel and oxidiser are fed to the RDE experimental rig using a series of pipes and hoses as part of the fuel and oxidiser feeding system.

2.3.2 RDE control system

The RDE control system used in this study integrates three subsystems, namely fuel-oxidiser feeding, ignition initiation and sequential control as presented in Figure 4. The control system was developed to simplify control, increase safety, and improve the success rate of the RDE operation. The fuel-oxidiser feeding system transports the designated gases from the gas storage room to the pre-detonator and RDE. There are numerous devices used for this RDE control system, such as solenoid valves, directional control valves, pneumatic valves, tubes, pipes, gas regulators, pressure gauges, flashback arrestors and flow meters. The summary of operating conditions used in the present study is presented in Table 2. Generally, there are two sets of fuel-oxidiser feeding lines that serve the pre-detonator and RDE separately. Flashback arrestors have been installed on each gas feed line to improve the safety of the experimental setup. In the present study, acetylene-oxygen and methane-oxygen were used as the fuel-oxidiser for the pre-detonator and RDE, respectively. The acetylene-oxygen mixture was chosen as the reactant for the pre-detonator as suggested by Mazlan et al. [36].

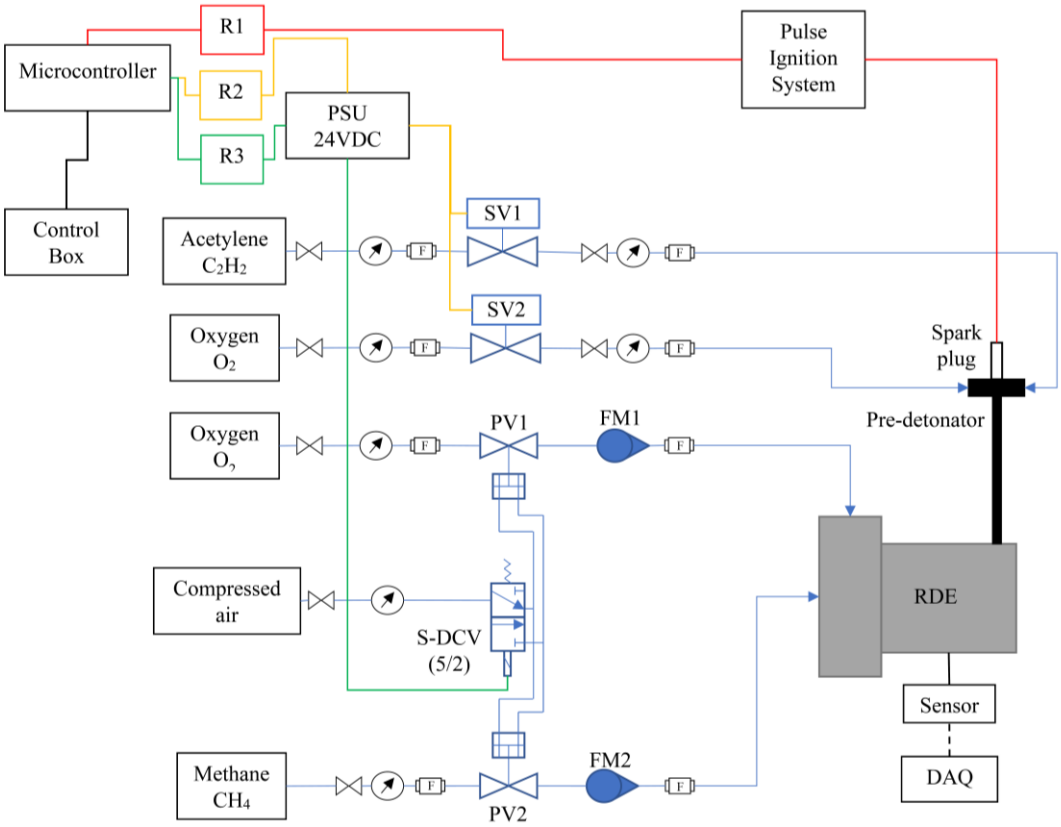

Figure 4. RDE control system comprises fuel-oxidiser feeding (blue line), ignition initiation (red line) and sequential control (green line)

Table 2. Summary of operating conditions used in the present study

Parameter	Value / Range
Pre-detonator fuel	Acetylene (C_2H_2)
Pre-detonator oxidizer	Oxygen (O_2)
RDE fuel	Methane (CH_4)
RDE oxidizer	Oxygen (O_2)
Equivalence ratio, φ	0.8 – 1.2
Total mass flow rate, $\dot{m}$total	3.8 – 4.2 kg/s
High-speed camera frame rate	150 000 fps
Image resolution	256 × 128
Exposure time	1 μs
Repetition per condition	3

The selection of an acetylene-oxygen mixture was made to ensure that optimal detonation propagation performance in the RDE can be achieved. The acetylene supply pressure was set at 1 bar to reduce the risk of rapid reaction in the present study. Meanwhile, methane was chosen as the reactant for the RDE combustion chamber due to its availability and low-cost energy sources [16]. The fuel-oxidiser mass flow rate for the RDE combustion chamber was set to 3.8 g/s, 4.0 g/s, and 4.2 g/s, with an equivalence ratio range of 0.8 to 1.2. In the meantime, the pre-detonator was set to a fuel-oxidiser mass flow rate of 1.4 g/s, with an equivalence ratio of 1.2. The fuel and oxidiser flow rates for both the pre-detonator and the small-scale RDE combustor were adjusted using variable-area flowmeters to achieve the required total mass flow rate and equivalence ratio. On the other hand, ignition during the RDE experiments was triggered by the ignition initiation system. The ignition initiation system consists of a pulse ignition module connected to the spark plug positioned at the top of the pre-detonator and linked to the RDE control panel. In addition, the ignition initiation system can be activated or deactivated via a single control switch, further enhancing its safety features. Meanwhile, the sequential control system manages the sequence of the RDE operation, including reactant feeding and ignition initiation. The activation of the components involved is controlled by a microcontroller connected to three relays, each responsible for managing a distinct operational function of the RDE. They are fuel-oxidiser feeding for the pre-detonator, for the RDE, and for ignition. Once the RDE operation is initiated at the control panel, the microcontroller will receive the signal and close the circuit for each RDE function accordingly. This will activate the solenoid valves for fuel-oxidiser feeding to the pre-detonator, the directional control valve for fuel-oxidiser feeding to the RDE combustion chamber, and the pulse ignition module.

Note that the activation of these RDE functions will follow the predefined sequence for RDE operation as shown in Figure 5. The sequence starts with the activation of both RDE and pre-detonator supply valves. After 'a' second, the pre-detonator supply valve will be closed, leaving the RDE supply valve to remain open. The ignition system will activate the pre-detonator after 'b' seconds, initiating the detonation wave from the pre-detonator into the RDE combustion chamber. Lastly, the supply valve for the RDE deactivated after 'c' seconds. The values for 'a', 'b' and 'c' can be modified and updated to the microcontroller. The values for 'a ', 'b' and 'c' were set to 100ms, 100ms and 600ms, respectively, in the present study.

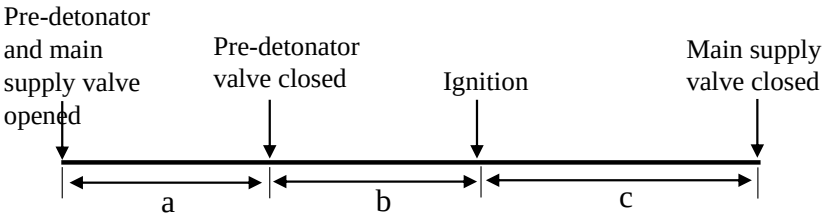

Figure 5. General predefined sequence of the RDE

2.3.3 RDE operation observation and high-speed imaging

Two network cameras, capable of capturing up to 1920×1080 resolution, were used to monitor the test room during the RDE experiments. One of the network cameras was placed diagonally facing the RDE exhaust, and the other was mounted on top of the test bed. In addition to monitoring the test room during experiments, the recorded footage is utilised to identify the exhaust flame plume during RDE operation. Other than that, high-speed imaging was used to visualise the propagation of the detonation wave during the RDE operation. The specifications of the high-speed camera used in the present study are summarised in Table 3. The high-speed camera is Phantom V710, which can capture a minimum resolution of 128 × 8 at 1,400,000 fps and a maximum resolution of 1200 × 800 at 7,500 fps. The high-speed camera is controlled via Phantom camera control and can record for up to 2.97s at the maximum frame rate. The lens used during the high-speed imaging is the Micro-Nikkor 105 mm f/2.8, a telephoto lens. This lens captured close-up shots from a safe distance and in dim lighting.

Table 3. Specifications of the high-speed camera used in the present study

Model	Vision Research, Phantom v710	
Main specifications	Resolution:	1280 × 800
	Sensor:	CMOS sensor
	Frame rate:	Over 7500 fps at full resolution Up to 1 400 000 fps at reduced resolutions
	Timing resolution:	better than 20ns
	Pixel depth:	8-bit and 12-bit

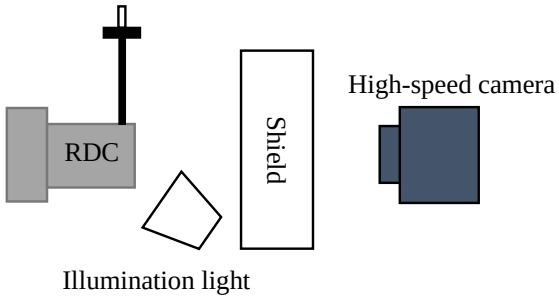

Figure 6. High-speed imaging arrangements

In the present study, the high-speed camera was set to capture at 150,000 fps with a resolution of 256 × 128 as described in Table 2. This setting has been chosen based on the acceptable image resolution and the ability to provide a sufficient frame rate that can track the movement of the wave propagating along the RDE circumference. The arrangement for the high-speed camera is shown in Figure 6. The illumination light was placed facing the RDE exhaust to enhance the ambient lighting. The high-speed camera was positioned facing the RDE annulus directly with transparent acrylic shields placed in between. This arrangement was made to protect the high-speed camera during the RDE operation from any impact produced by the shock waves.

Furthermore, the wave propagation velocity based on the high-speed images was estimated from the time required for the luminous front to complete one full revolution around the small-scale RDE annulus. In the present study, the wave propagation circumferential path was determined using the mean annulus diameter, since the propagating luminous front was assumed to travel approximately within the middle region of the annular channel. This assumption is consistent with previous studies, which reported that the wave in an RDE propagates approximately along the annulus's mean diameter [38]–[40]. Accordingly, the wave propagation velocity was estimated from $v = \pi D_m/(N\Delta t)$, where D_m is the mean annulus

diameter, N is the number of frames required for one full revolution, and Δt is the frame interval corresponding to the high-speed camera frame rate [24]. The image scale was based on the known combustor annulus geometry visible in the recorded image. The main source of uncertainty in the present wave propagation velocity estimation based on the high-speed images was assumed to arise from visual identification of the luminous front position and the exact frame corresponding to one complete revolution. A frame count uncertainty of approximately ±1 frame was considered and corresponds to an estimated relative uncertainty of about ±6% for the typical revolution count of 17 to 18 frames observed in the present study. The reported values were further improved through repeated inspections at multiple positions within each image sequence and repeated hot tests for each operating condition. In addition to the image-based measurement limitations, several constraints in the current experimental setup for the small-scale RDE should also be noted. Specifically, the injector pressure ratio, discharge coefficient, actual injector exit velocity, plenum pressure, and injector pressure drop were not directly measured or recorded, thereby limiting the completeness of the experimental characterisation. Additionally, the reactants, such as methane and oxygen, were supplied separately in a non-premixed manner and combined immediately before entering the annular combustion chamber. The homogeneity of the resulting mixture was not directly assessed, which represents another limitation in the study of small-scale RDE performance.

In earlier work, the pressure-related behaviour of the present small-scale RDE configuration was investigated using high-frequency pressure diagnostics [30]. The earlier study described the pressure instrumentation and acquisition setup. In addition, the recorded pressure traces and Fast Fourier Transform (FFT) spectra were used to characterise the chamber-pressure behaviour, dominant frequency characteristics, and instability features of the small-scale RDE over the tested equivalence-ratio range. Accordingly, the present manuscript does not repeat the earlier pressure-based results but focuses on the optical wave propagation characteristics obtained from high-speed imaging. It should be emphasised that luminosity tracking alone does not establish the proof of detonation. Therefore, the luminous fronts observed in the present study are interpreted alongside the previously reported pressure-based characterisation of the same RDE configuration. It should also be noted that the earlier pressure study was limited to a single annulus measurement location and did not provide full spatial pressure resolution along the combustor.

3. Results and Discussion

The pressure-based behaviour of the present small-scale RDE configuration within the tested equivalence-ratio range has been reported previously [30], including high-frequency pressure traces, FFT-based frequency characteristics, and instability features under a constant total mass flow rate. The previous study indicated unstable operating behaviour, primarily in the form of chaotic and waxing-and-waning instabilities, with the least instability observed near the balanced-mixture condition. In the present study, high-speed imaging observations are discussed in relation to previously reported pressure-based findings to more consistently interpret the observed luminous-front behaviour. However, the exact timing of the local wave discontinuity, the detailed pressure-wave sequence along the combustor, and the full spatial development of the instability cannot be resolved from the present optical measurements alone, whereas the previous pressure-based study was restricted to a single annulus pressure-measurement location. The experimental results presented in this study include RDE initiation using a pre-detonator, flame plume characteristics and wave propagation characteristics. Furthermore, the extracted results from the high-speed images, such as wave propagation velocity and frequency, are discussed as follows.

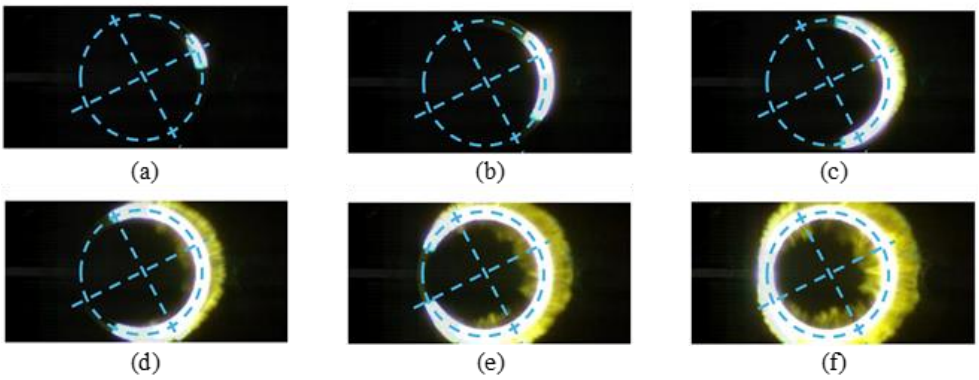

Figure 7. Pre-detonator initiation, detonation wave propagation

3.1 RDE Initiation Using Pre-Detonator

Investigations into the initiation characteristics via the pre-detonator were conducted using high-speed imaging. Figure 7 shows high-speed image frames capturing the initial propagation of the starting combustion front around the RDE annulus and subsequent events. The RDE combustion chamber was observed to be directly initiated by the pre-detonator with two concurrent detonation waves propagated around the RDE annulus in opposite directions. These detonation waves then intersected and merged on the opposite side of the annulus, as shown in Figure 7(f). In addition, the clockwise detonation wave was observed to be more dominant, as it propagates faster than the counterclockwise one. A study by Mizener [41], who has found a similar phenomenon, reported that these concurrent waves appear as self-cancelling waves.

3.2 Flame Plume Characteristics

In the present study, the flame plume was captured using the network camera and considered as low-speed video observations. Although the visual quality produced by the network camera was slightly inferior, the resulting images can still be used to understand the situation.

Table 4–6 show the flame plume for total mass flow rates ($\dot{m}_{total}$) of 3.8 g/s, 4.0 g/s, and 4.2 g/s, respectively. The side-view images were taken by the network camera placed diagonally facing the RDE exhaust. Meanwhile, the top-view images were captured by the network camera mounted on top of the test bed. It should be noted that the flame plume images presented in the present study are used only for qualitative observation of the external combustion behaviour and are not employed for quantitative parameter extraction.

Table 4. Flame plume for $\dot{m}_{total}$=3.8g/s

	$\dot{m}_{total}$ = 3.8g/s				
	EQUIVALENCE RATIO				
	0.8	0.9	1.0	1.1	1.2
SIDE VIEW					
TOP VIEW					

Table 5. Flame plume for $\dot{m}_{total}$=4.0g/s

	$\dot{m}_{total}$ = 4.0g/s				
	EQUIVALENCE RATIO				
	0.8	0.9	1.0	1.1	1.2
SIDE VIEW					
TOP VIEW					

As can be seen, the flame plume from the RDE exhaust shows the bright white of the methane-oxygen flame. The flame was observed to become dimmer and less distinct as the equivalence ratio decreased, approaching the fuel-lean condition. Furthermore, flames with yellow-orange regions were found to increase in visibility and size as the equivalence ratio increased. A comparable scenario was reported by Mizener [41] for a hydrogen-oxygen flame, with additional observation found a more transparent flame as the equivalence ratio decreases. It is noted that the composition of fuel is increased, and the composition of the oxidiser decreases with respect to the equivalence ratio increment. Thus, more complete combustion may occur at a lower equivalence ratio than in more fuel-rich conditions. When excessive fuel content is present during RDE operation, incomplete combustion may occur, leaving yellow-orange colour traces in the flame plume.

Resembling characteristics were observed across variations in the equivalence ratio (0.8 to 1.2) for the cases with $\dot{m}_{total}$ = 4.0 g/s and $\dot{m}_{total}$ = 4.2 g/s. Further investigations into different total mass flow rates have shown that flame plume visibility and size increase with higher total mass flow rates. The yellow-orange colour regions of the flame were observed to be more pronounced at higher total mass flow rates, consistent with a study by Law et al. [11], especially for equivalence ratios of 1.1 and 1.2. The fuel composition is lower at a lower total mass flow rate at a given equivalence ratio, leading towards more complete combustion. As the total mass flow rate increases, the dynamics of the flow characteristics within the combustor intensify, increasing the dominant flow-field frequency and thereby enhancing the flame intensity. The appearance of a yellow-orange flame at the RDE exhaust, particularly at higher total mass flow rates and richer equivalence ratios, may indicate that part of the reactant mixture was not completely burned in the combustor and continued to react downstream of the exhaust. Besides brightness, no other significant differences or phenomena were

observed, such as a Mach disc or a weak shock train, as reported by Stechmann [22] for RDE with a straight nozzle. This may be due to the footage being illuminated during the RDE experiment and to the low total mass flow rates used as operating conditions. In addition, the straight nozzle represents the RDE annulus with no area change. It was said that the alteration of the supersonic flow field after the RDE exit can be achieved by adding nozzles, such as a divergent nozzle or a convergent-divergent nozzle [42]. The divergent nozzle produces an expanding area, and the convergent-divergent nozzle has both convergent and divergent areas. RDE with this extension, such as the aerospike nozzle, has been reported to produce a strong shock train as the shock emerging from the nozzle tip is recompressed [22].

Table 6. Flame plume for $\dot{m}_{total}$=4.2g/s

	$\dot{m}_{total}$ = 4.2g/s.				
	EQUIVALENCE RATIO				
	0.8	0.9	1.0	1.1	1.2
SIDE VIEW					
TOP VIEW					

3.3 Wave Propagation Characteristics

High-speed videography and imaging with a high-speed camera were used to visualise the wave propagation characteristics during operation of the present small-scale RDE. The position of the propagating luminous front at each instant can be traced from the high-luminosity regions within the RDE flow field. Furthermore, high-speed imaging can be used to observe wave dynamics, such as the emergence and disappearance of multiple luminous fronts, and to directly estimate the wave propagation speed. In the present study, the high-speed camera was placed approximately 1.5m facing the small-scale RDE exhaust to capture the entire annulus image. Figure 8 shows a sample of the wave propagation images for the case of $\dot{m}_{total}$ = 3.8g/s at three different equivalence ratios representing fuel-lean (φ = 0.8), stoichiometric (φ = 1.0) and fuel-rich (φ = 1.2) conditions. The visual representations obtained from the small-scale RDE annulus show noticeable differences when compared across different equivalence ratios. At an equivalence ratio of 0.8, faint luminosity associated with wave propagation was observed compared with the other equivalence ratios. The luminosity of the propagating front increased with the equivalence ratio. For the fuel-lean and stoichiometric cases, the wave propagation structure could still be characterised by a relatively clear peak-luminosity region followed by a decay phase. However, in the fuel-rich case, the peak luminosity region appeared less well-defined, as it was followed by a brighter decay zone. These observations were consistent with a study by Stechmann [22]. Further analysis of the wave propagation characteristics was also conducted for different total mass flow rates. A higher total mass flow rate may indirectly increase the pressure level within the RDE annulus, leading to higher luminosity of the propagating front. This behaviour may also be associated with the higher fuel supply at a higher total mass flow rate for the same equivalence ratio, resulting in a greater heat release.

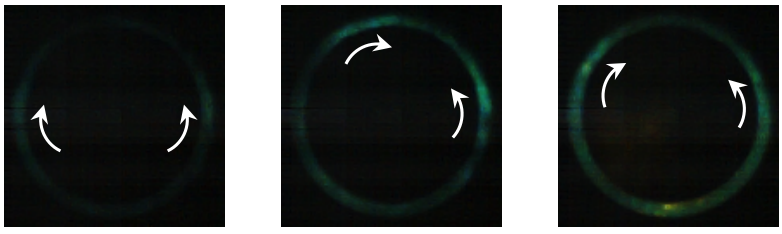

(a) (b) (c)

Figure 8. Wave propagation for $\dot{m}_{total}$ = 3.8g/s with equivalence ratio (a) 0.8, (b) 1.0, and (c) 1.2

Throughout the small-scale RDE operation, the luminous wavefront propagating along the annulus was observed to alternate between single-wave and dual-wave behaviour, as shown in Figure 9 and Figure 10, respectively. For the dual-wave case, one luminous front was observed to be brighter than the other and may be considered as the dominant front in terms of luminosity. One possible explanation for the appearance of multiple propagating fronts has been described by Anand [42], who suggested that a propagating front may become slanted toward the fuel-oxidiser feeding location. Under these conditions, the fresh reactants may enter the oblique shock structure associated with the leading front and cause autoignition that may contribute to the appearance of a second propagating front. Nevertheless, the interpretations in the

present study remain qualitative because the high-speed images obtained are unable to provide the full wave structure during the small-scale RDE operation.

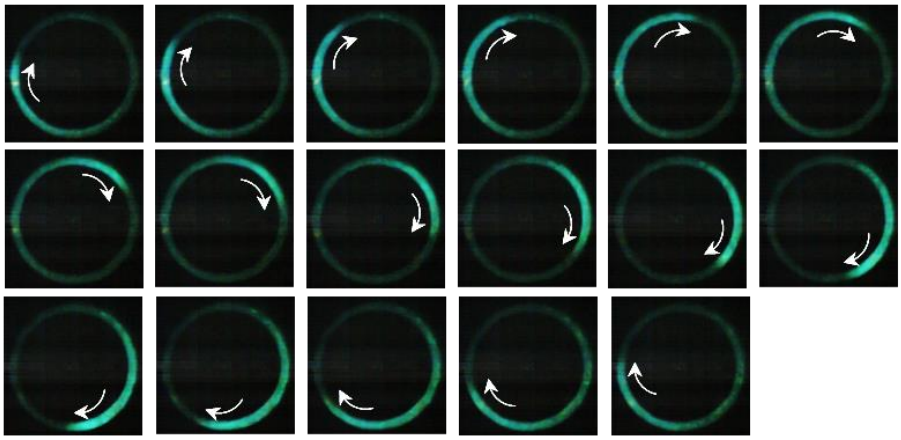

Figure 9. Single-wave propagation during small-scale RDE operation for $\dot{m}$ = 4.2g/s and equivalence ratio 1.1

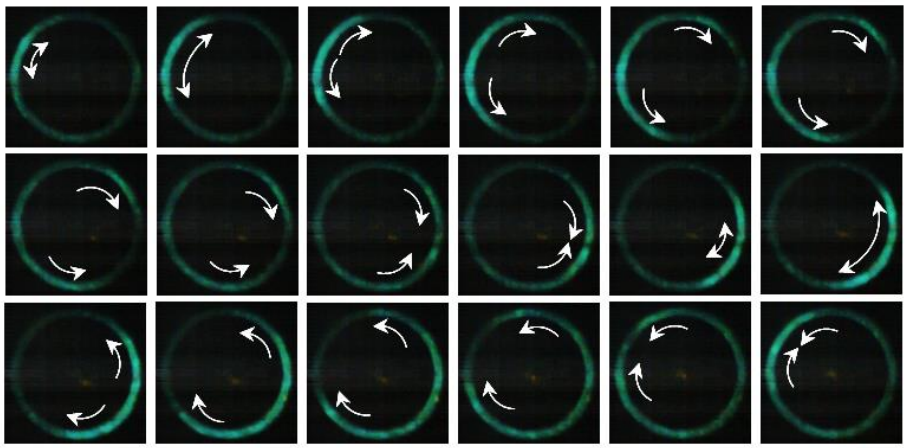

Figure 10. Dual-wave propagation during small-scale RDE operation for $\dot{m}$ = 4.2g/s and equivalence ratio 1.1

Since both single-wave and dual-wave propagation were observed under all tested conditions in the present study, no clear dependence of the observed wave pattern on the total mass flow rate could be established within the investigated operating range. Although previous studies, such as those conducted by Bykovskii et al. [21], have reported that the number of waves may increase with increasing mass flow rate and pressure, the present findings were found to be more comparable to the study by Stechmann [22], which reported that the number of observed waves is independent of mean chamber pressure and mass flow rate. This situation may be related to the small pressure variation resulting from low total mass flow rates and the unchoked exhaust condition during the blowdown process examined in the present study. In addition, a large pressure rise associated with the propagating wave may reduce or temporarily block the fresh reactant supply as the wave passes over the injectors during the RDE operation [43]. Consequently, the presence of propagating fronts, especially in multiple-wave propagation, may alter the injector recovery timing and affect the fuel-oxidiser mixing process. These situations can degrade the quality of the reaction process, such as reducing the participation of fresh reactants or increasing secondary losses due to insufficient replacement of fresh reactants in the annulus. Furthermore, the high-speed image sequences revealed that even under identical operating conditions, the luminous front could alternate between a single front and two fronts propagating in opposite circumferential directions. This indicates that both single-wave and dual counter-rotating wave behaviours occurred in the small-scale RDE under the investigated operating conditions. The high-speed images further suggest interaction between the opposing wavefronts within the annulus, although the exact collision location and timing could not be determined precisely from the present images. Generally, these observations are consistent with the instability characteristics as reported in the previous work for the same small-scale RDE configuration using high-frequency pressure diagnostics, in which unstable wave behaviour and irregularities were identified [30].

3.4 Wave Propagation Velocity and Wave Propagation Frequency

Subsequently, the wave propagation velocity and frequency have been estimated from high-speed image sequences obtained during the experiment. The time interval between consecutive frames was determined to be 6.67×10^{-6} s, corresponding to the high-speed camera frame rate of 150,000 fps. Accordingly, the wave propagation velocity and frequency were determined by visually tracking the number of frames required for the luminous front to complete one full revolution around the annulus circumference based on the mean annulus diameter of 42mm. It should be noted that the detonation wave in RDE typically propagates along the mean diameter of the annulus [38 – 40], and a similar image-

based tracking approach has been reported by previous researchers [24]. The experiments for each equivalence ratio (φ = 0.8–1.2) and total mass flow rate ($\dot{m}_{total}$ = 3.8 g/s, 4.0 g/s, 4.2 g/s) were repeated three times, resulting in a total of 45 hot tests in the present study. To improve the reliability of the extracted results, each video was visually inspected at three different positions within the middle one-third segment of the actual hot-test period in the combustor. This approach was adopted to minimise the influence of the strong impulse immediately after initiation [10] and the significant flow-rate variation toward the end of the test [12]. Additionally, the interval between visually inspected positions was approximately 10,000 frames, equivalent to 66.7ms. The wave propagation velocity and frequency values were then averaged, as presented in Figure 11 and 12, respectively.

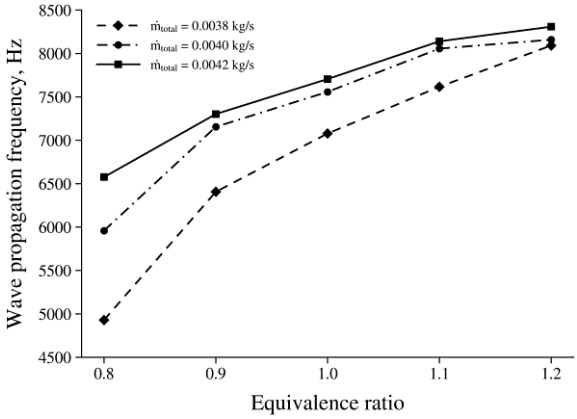

Figure 11. Wave propagation frequency for different total mass flow rates with respect to the equivalence ratio

As reported by Rankin et al. [4], rotating-wave propagation behaviour is influenced by factors such as fuel composition, equivalence ratio, and combustor geometry. In the present study, the average wave propagation frequency shown in Figure 11 increased as the equivalence ratio increased for a given total mass flow rate. The lowest and highest average wave propagation frequencies were approximately 4900 Hz and 8300 Hz, observed at φ = 0.8 and $\dot{m}_{total}$ = 3.8 g/s, and at φ = 1.2 and $\dot{m}_{total}$ = 4.2 g/s, respectively. Since the propagation frequency is directly related to the time required for the luminous front to complete one annulus revolution, higher propagation frequencies resulted in higher estimated propagation velocities. The estimated wave propagation frequencies in the present study are significantly higher than the typical operating frequencies reported for PDE and are more consistent with the higher-frequency operating behaviour associated with RDE.

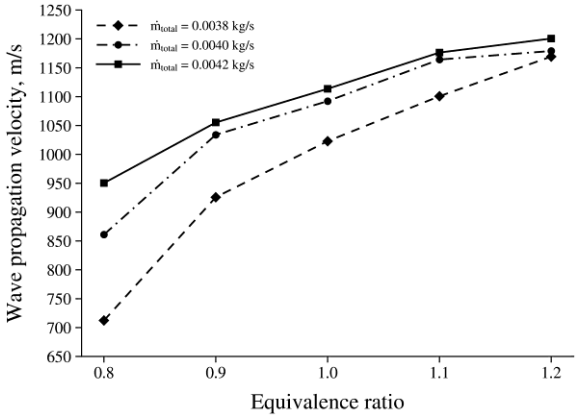

Figure 12. Wave propagation velocity at different equivalence ratios and total mass flow rates

In addition to the wave propagation frequency, the average wave propagation velocity during the small-scale RDE operation was estimated from the high-speed images. For $\dot{m}_{total}$ = 3.8g/s, the average wave propagation velocity at φ = 0.8, 0.9, 1.0, 1.1, and 1.2 was 712m/s, 925m/s, 1022m/s, 1100m/s and 1169m/s, respectively. For $\dot{m}_{total}$ = 4.0g/s, the corresponding values were 861m/s,1033 m/s,1092 m/s,1164 m/s and 1179.4m/s, respectively. Meanwhile, for $\dot{m}_{total}$ = 4.2g/s, the average wave propagation velocity was 950m/s, 1055m/s, 1113m/s, 1176m/s, and 1200m/s for φ = 0.8, 0.9, 1.0, 1.1, and 1.2, respectively. As shown in Figure 13, all measured wave propagation velocities were noticeably lower than the calculated ideal Chapman-Jouguet detonation wave velocity (U_{CJ}). The average wave propagation velocities measured for $\dot{m}_{total}$ of 3.8g/s, 4.0g/s and 4.2g/s determined in this study were found to fall within 31 -47%, 37 - 47% and 41 - 48% of the calculated ideal U_{CJ}, respectively.

This significant difference may be associated with non-ideal wave behaviour under very low-flow-rate operation, including incomplete reactant replenishment, inhomogeneous mixing, and unstable propagation characteristics in the short annular combustor of a small-scale RDE. The condition of the fresh reactants immediately ahead of the propagating wave front is known to influence the propagation process [44]. A shorter circumferential path in the small-scale annular

RDE combustor reduces the available time for injector recovery, reactant refilling, and fuel-oxidiser mixing before the next wave propagation cycle. This may contribute to the significant wave-propagation velocity deficit relative to the U_{CJ} observed in all cases in the present study. As described by Xu et al. [45], a higher wave propagation velocity can be obtained by a larger rotating detonation combustor, which provides a longer recovery and mixing period. Such non-ideal behaviour may also involve post-front heat release caused by secondary combustion processes, including parasitic and commensal combustion, which may arise from incomplete and unsteady mixing of fuel and oxidiser [16], [46]- [47]. This may result in additional heat release behind the main propagating front, thus weakening the effective pressure-gain process and reducing the overall detonation efficiency. On the other hand, a similar trend in wave propagation velocity, as reported by Russo et al. [2] and Guo et al. [48], was observed: the wave propagation velocity increased with increasing equivalence ratio at a given total mass flow rate. For all tested total mass flow rates in the present study, the lowest wave propagation velocity was observed at $\varphi = 0.8$, while the highest was at $\varphi = 1.2$. Within the equivalence ratio range investigated in the present study, this trend may be associated with stronger overall heat release and luminous propagation behaviour as the mixture approached richer conditions [45]. However, several previous studies, including Xu et al. [45] and Jing and Ma [49], have reported that the wave propagation velocity may increase initially and then decrease beyond a certain equivalence ratio. The maximum wave propagation velocity often occurs near the stoichiometric equivalence ratio.

According to Jing and Ma [49], this phenomenon is attributed to the fuel and oxidiser content. Under fuel-lean conditions, the oxidiser content can be considered as higher than the fuel and sufficient to ensure complete combustion. Therefore, the velocity of wave propagation increases, and the intensity increases as the equivalence ratio approaches the stoichiometric equivalence ratio. As the equivalence ratio increases further toward fuel-rich conditions, the oxidiser composition continues to decrease, limiting the reaction stoichiometry and causing incomplete combustion, which reduces the wave propagation intensity and velocity.

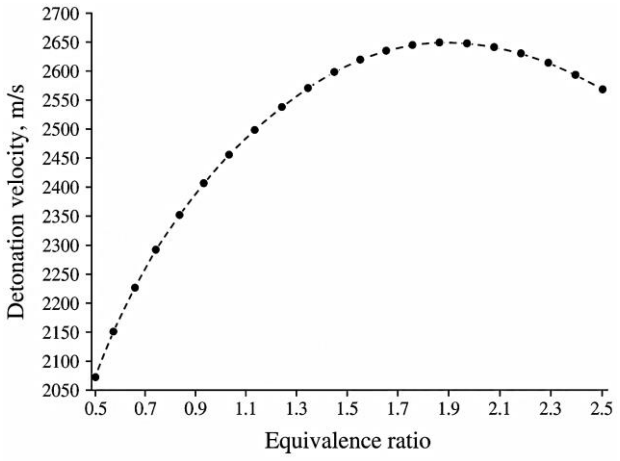

Figure 13. U_{CJ} from NASA CEA program

Figure 13 shows the U_{CJ} determined using the NASA CEA program for a methane-oxygen mixture at an initial pressure of 1.45 bar over the equivalence ratio range $\varphi = 0.5$ - 2.5. The initial pressure used in the NASA CEA estimation corresponds to the combustor pressure during the reactant feeding process before ignition. As shown in Figure 13, the U_{CJ} increased as the equivalence ratio increased from 0.5 to 1.9, reaching a maximum near $\varphi = 1.9$, then decreased with further increases in the equivalence ratio. Since the maximum equivalence ratio investigated experimentally in the present study was $\varphi = 1.2$, the operating range may not have reached the equivalence ratio corresponding to the maximum ideal detonation velocity predicted by NASA CEA. Nevertheless, a gradual increase in the experimentally estimated wave propagation velocity beyond the stoichiometric conditions could still be observed, especially for $\dot{m}_{total} = 4.0$g/s and $\dot{m}_{total} = 4.2$ g/s. The wave propagation frequency and velocity were also found to increase with increasing total mass flow rate at a given equivalence ratio. This observation is consistent with Han et al. [10], who also reported that detonation speed may increase slightly as chamber stagnation pressure rises with increasing total mass flow rate. In the present study, a higher mass flow rate, which is generally associated with a higher injection pressure, may improve the condition of the fresh reactants supplied immediately ahead of the propagating front and influence the wave propagation behaviour [44]. On the other hand, although increasing the equivalence ratio was associated with higher wave propagation velocity in the present study, previous work has shown that richer-fuel operation may also reduce overall stability [50]. Additionally, as the oxidiser flow rate increases, reactant mixing quality may deteriorate due to higher annulus flow velocity and reduced residence time of the reactant mixture [51]. Therefore, achieving an appropriate balance among the chemical composition of the reactants, oxidiser flow conditions, and mixing quality is essential to sustain stable and repeatable wave propagation during small-scale RDE operation. Overall, the high-speed image analysis in the present study indicates that equivalence ratio and total mass flow rate influenced the observed wave propagation behaviour of the small-scale RDE. Although the present dataset does not allow a full scaling-law analysis, the observed propagation behaviour can still be discussed quantitatively using the measured wave propagation frequency and velocity, and by comparison with the ideal U_{CJ}. However, the present approach is limited to visualising the luminous front and cannot fully identify all instability types.

4. Conclusions

In this study, high-speed imaging was used to examine the initiation process, flame plume behaviour, and luminous wave propagation characteristics in a small-scale RDE operating with methane–oxygen mixtures. The effects of equivalence ratio and total mass flow rate on the observed propagation behaviour were analysed. The main findings of the present study are as follows:

- During initiation using the pre-detonator, two luminous fronts propagating in opposite circumferential directions were observed within the annular chamber. In several cases, one front appeared more dominant than the other based on the image sequence.
- The flame plume under fuel-rich conditions exhibited a more pronounced yellow-orange luminous region at the exhaust, which became increasingly visible as the equivalence ratio increased. This behaviour was also more noticeable at higher total mass flow rates, which may be associated with reduced reactant residence time and non-ideal mixing.
- Higher wave luminosity was observed at higher total mass flow rates. This characteristic suggests a stronger luminous combustion response under these conditions, although the present high-speed image data do not provide direct confirmation on the chamber pressure or detailed thermodynamic behaviour.
- The average wave propagation velocity obtained in the present study was lower than the calculated ideal U_{CJ} for all tested cases. The measured wave propagation velocities were approximately 31–48% of the ideal U_{CJ} values. The velocity deficit may be associated with non-ideal wave propagation under very low-flow-rate operation, including incomplete mixing, limited replenishment of the reactant mixture, and instability effects.
- The measured wave propagation frequency was higher than the typical operating frequency range of the PDE, indicating the high-frequency nature of the present rotating-wave process. In general, the observed propagation frequency and wave propagation velocity showed an interrelated trend across the tested conditions.

Overall, the present study provides a qualitative and semi-quantitative assessment of wave propagation behaviour in a small-scale RDE under low total mass-flow-rate operation. However, the conclusions of this work should be interpreted in light of its limitations. Since the present study relied primarily on high-speed imaging, the detailed detonation structure, transient thrust behaviour and full pressure-wave dynamics could not be established only from the present dataset. Further investigations should combine synchronised measurements of multiple high-frequency pressure signals, direct thrust measurements, and optical diagnostics to achieve a more comprehensive understanding and higher-resolution view of the transient behaviour in small-scale RDE operation. Future studies should also examine the emissions characteristics, overall efficiency, inlet-orifice effects, and the influence of choked and unchoked operating conditions to support a more extensive performance evaluation.

Acknowledgements

We would like to thank and acknowledge Universiti Teknologi Malaysia Pahang Al-Sultan Abdullah (UPNM) for funding this project.

Funding

The research was supported by Universiti Teknologi Malaysia through the High Impact Research Grant with cost centre number Q.J130000.2451.09G05.

Declaration of Competing Interest

The author declares no conflicts of interest.

CRediT Authorship Contribution Statement

Mohd Fahmi Md Salleh: Methodology, Investigation, Writing – original draft
Mazlan Abdul Wahid: Conceptualisation; Supervision; Funding acquisition, Writing – review & editing
Hussein A. Mohammed: Analysis; Writing – review & editing
Natrah Kamaruzaman: Conceptualisation; Supervision; Writing – review & editing
Umar Ikhwan Mohd Rozaiddin: Methodology; Writing – review & editing
Ahmad Dairobi Ghazali: Methodology; Writing – review & editing

Availability of Data and Materials

The data supporting this study's findings are available on request from the corresponding author.

Ethics Declarations

This study did not involve human participants or animals. Ethical approval was therefore not required.

Generative Artificial Intelligence Declarations

The authors claim that artificially intelligent-assisted technologies, such as generative AI, were not used to generate content, ideas, or theories. We have just utilised AI to enhance readability and refine the language. This was used with extreme human control and oversight. The authors take full responsibility for reviewing and approving the content.

References

[1] R. Zhou, D. Wu, and J. Wang, "Progress of continuously rotating detonation engines," *Chinese Journal of Aeronautics*, vol. 29, no. 1, pp. 15–29, 2016.

[2] R. M. Russo, P. I. King, F. R. Schauer, and L. M. Thomas, "Characterization of pressure rise across a continuous detonation engine," in *47th AIAA/ASME/SAE/ASEE Joint Propulsion Conference and Exhibit*, 2011.

[3] H. Liu, F. Song, D. Jin, S. Xu, and X. Yang, "Experimental investigation on spray and detonation initiation characteristics of premixed/non-premixed RDE," *Fuel*, vol. 331, p. 125949, 2023.

[4] B. A. Rankin, D. R. Richardson, A. W. Caswell, A. Naples, J. L. Hoke, and F. R. Schauer, "Imaging of OH* chemiluminescence in an optically accessible nonpremixed rotating detonation engine," in *53rd AIAA Aerospace Sciences Meeting, 2015, American Institute of Aeronautics and Astronautics Inc, AIAA*, 2015.

[5] G. D. Roy, S. M. Frolov, A. A. Borisov, and D. W. Netzer, "Pulse detonation propulsion: Challenges, current status, and future perspective," *Progress in Energy and Combustion Science*, vol. 30, no. 6, pp. 545-672, 2004.

[6] C. Yang, X. Wu, H. Ma, L. Peng, and J. Gao, "Experimental research on initiation characteristics of a rotating detonation engine," *Experimental Thermal and Fluid Science*, vol. 71, pp. 154–163, 2016.

[7] I. J. Shaw, J. A.Kildare, M. J. Evans et al. A theoretical review of rotating detonation engines. *Direct Numerical Simulations-An Introduction and Applications*, 2019.

[8] J. Hu and B. Zhang, "Time/frequency domain analysis of detonation wave propagation mechanism in a linear rotating detonation combustor," *Applied Thermal Engineering*, vol. 255, p. 124014, 2024.

[9] O. Venegas, C. Hernández, and C. Fernández, "Review on the fundamentals and recent developments in rotating detonation engines experimental and numerical setups," *Propulsion and Power Research*, vol. 14, no. 4, pp. 595–610, 2025.

[10] H. S. Han, E. S. Lee, and J. Y. Choi, "Experimental investigation of detonation propagation modes and thrust performance in a small rotating detonation engine using C_2H_4 /O_2 propellant," *Energies* (Basel)., vol. 14, no. 5, p. 1381, 2021.

[11] H. Law, T. Baxter, C. Ryan, and R. Deiterding, "Design and testing of a small-scale laboratory rotating detonation engine running on ethylene-oxygen," in *AIAA Propulsion and Energy Forum, 2021, American Institute of Aeronautics and Astronautics Inc, AIAA*, 2021.

[12] W. Armbruster et al., "Experimental investigation of a small-scale oxygen-hydrogen rotating detonation rocket combustor," in *AIAA SciTech Forum and Exposition*, 2024.

[13] A. Dairobi G, M. A. Wahid, M. A. Mazlan, and M. H. Azeman, "Early assessment of asymmetric vortex small rotating detonation engine," *Evergreen*, vol. 8, no. 1, pp. 182–186, 2021.

[14] J. R. Dechert, F. Schauer, M. D. Polanka, S. A. Schumaker, B. C. Sell, and M. L. Fotia, "Development of a small-scale rotating detonation engine," in *AIAA Scitech 2020 Forum, American Institute of Aeronautics and Astronautics Inc, AIAA*, 2020, pp. 1–11.

[15] Y. Kudo, Y. Nagura, J. Kasahara, Y. Sasamoto, and A. Matsuo, "Oblique detonation waves stabilized in rectangular-cross-section bent tubes," *Proceedings of the Combustion Institute*, vol. 33, no. 2, pp. 2319–2326, 2011.

[16] S. Prakash, V. Raman, C. F. Lietz, W. A. Hargus, and S. A. Schumaker, "Numerical simulation of a methane-oxygen rotating detonation rocket engine," in *Proceedings of the Combustion Institute*, Elsevier, pp. 3777–3786, 2021.

[17] K. J. Durkee, R. T. Dave, M. Maybee, G. R. Cobb, J. R. Burr, and J. W. Bennewitz, "Performance comparison of variable center body configurations for a 25 mm rotating detonation rocket engine," in *AIAA SCITECH 2025 Forum, in AIAA SciTech Forum, American Institute of Aeronautics and Astronautics*, 2025.

[18] R. T. Dave, K. J. Durkee, M. A. Maybee, G. R. Cobb, J. R. Burr, and J. W. Bennewitz, "Experimental testing of a 25 mm rotating detonation rocket engine with methane and hydrogen," in AIAA Science and Technology Forum and Exposition, AIAA SciTech *Forum*, 2025.

[19] T. Mundt, C. Knowlen, and M. Kurosaka, "Scale effects on rotating detonation rocket engine operation," *Applications in Energy and Combustion Science*, vol. 19, p. 100282, 2024.

[20] R. Yokoo et al., "Combustion pressure distributions and thrust performances in small cylindrical rotating detonation engines," in *AIAA Scitech 2020 Forum, American Institute of Aeronautics and Astronautics Inc, AIAA*, 2020.

[21] F. A. Bykovskii, S. A. Zhdan, and E. F. Vedernikov, "Continuous spin detonations," *Journal of propulsion and power*, vol. 22, no. 6, pp. 1204–1216, 2006.

[22] D. P. Stechmann, "*Experimental study of high-pressure rotating detonation combustion in rocket environments*," Doctor of Philosophy, Purdue University, Indiana, 2017.

[23] V. Anand, A. George, R. Driscoll, and E. Gutmark, "Analysis of air inlet and fuel plenum behavior in a rotating detonation combustor," *Experimental Thermal and Fluid Science*, vol. 70, pp. 408–416, 2016.

[24] P. K. Keller, M. D. Polanka, F. R. Schauer, J. J. Wyatt, and B. C. Sell, "Low mass-flow operation of small-scale rotating detonation engine," *Applied Thermal Engineering*, vol. 241, p. 122352, 2024.

[25] H. Xu, F. Wang, Y. Wu, and C. Weng, "Investigation into the instability mechanism of hydrogen-oxygen rotating detonation wave propagation using a small-scale model," *Baozha Yu Chongji/Explosion and Shock Waves*, vol. 45, no. 1, pp. 012101-1, 2025.

[26] S. Valencia, A. Mendiburu, L. Bravo, P. Khare, and C. Celis, "Flow-field analysis and performance assessment of rotating detonation engines under different number of discrete inlet nozzles," *Applications in Energy and Combustion Science*, vol. 20, p. 100296, 2024.

[27] A. Pallela and A. K. Thakur, "Numerical evaluation of quiescent mixtures suitable for a sustainable detonation in pulse detonation engine," *Aerospace Systems*, pp. 1-14, 2025.
[28] H. Wang and M. A. Oehlschlaeger, "," *International Journal of Chemical Kinetics*, vol. 52, no. 10, 2020.
[29] T. Sato, F. Chacon, M. Gamba, and V. Raman, "Mass flow rate effect on a rotating detonation combustor with an axial air injection," *Shock Waves*, vol. 31, no. 7, pp. 741–751, 2021.
[30] M. F. Md Salleh, "Experimental Investigation on Shock tube ignition delay time measurements for methyl propanoate and methyl acrylate: Influence of saturation on small methyl ester high-temperature reactivity performance characteristics of a small-scale rotating detonation engine," *Journal of Mechanical Engineering*, vol. 23, no. 1, pp. 84–100, 2026.
[31] I. V Walters, A. Lemcherfi, R. M. Gejji, S. D. Heister, and C. D. Slabaugh, "Performance characterization of a natural gas-air rotating detonation engine," *Journal of Propulsion and Power*, vol. 37, no. 2, pp. 292–304, 2021.
[32] K. Malik, M. Żbikowski, and A. Teodorczyk, "Detonation cell size model based on deep neural network for hydrogen, methane and propane mixtures with air and oxygen," *Nuclear Engineering and Technology*, vol. 51, no. 2, pp. 424–431, 2019.
[33] M. N. Rahman, "*Numerical analysis of detonation stability in a rotating detonation engine fueled with biogas and hydrogen*," Doctoral dissertation, Universiti Teknologi Malaysia, Malaysia, 2021.
[34] J. Kindracki, P. Wolański, and Z. Gut, "Experimental research on the rotating detonation in gaseous fuels-oxygen mixtures," *Shock Waves*, vol. 21, no. 2, pp. 75–84, 2011.
[35] M. A. Mazlan, M. F. M. Yasin, A. Saat, M. A. Wahid, A. D. Ghazali, and M. N. Rahman, "Initiation characteristics of rotating supersonic combustion engine," *Evergreen*, vol. 8, no. 1, pp. 177–181, 2021.
[36] M. A. Mazlan, M. F. M. Yasin, A. Saat, M. A. Wahid, A. D. Ghazali, and H. Azeman, "Wave propagation characteristics in predetonator of rotating detonation engine," *AIP Conference Proceedings*, vol. 2749, no. 1, p. 70009, 2023.
[37] Department of occupational safety and health, guidelines on storage of hazardous chemicals: A guide for safe warehousing of packaged hazardous chemicals. Ministry of Human Resources Malaysia, 2006.
[38] V. R. Katta, K. Y. Cho, J. L. Hoke, J. R. Codoni, F. R. Schauer, and W. M. Roquemore, "Effect of increasing channel width on the structure of rotating detonation wave," *Proceedings of the Combustion Institute*, vol. 37, no. 3, pp. 3575–3583, 2019.
[39] N. Zhao, Q. Meng, H. Zheng, Z. Li, and F. Deng, "Numerical study of the influence of annular width on the rotating detonation wave in a non-premixed combustor," *Aerospace Science and Technology*, vol. 100, p. 105825, 2020.
[40] R. S. Sidorov, "Numerical investigation of the operating process in an annular detonation chamber of low diameter," in *Journal of Physics: Conference Series*, vol. 1675, no. 1, p. 012065, 2020.
[41] Andrew R. Mizener, "*Performance modelling and experimental investigations of rotating detonation engines*," Doctor of Philosophy, The University of Texas at Arlington, Texas, 2018.
[42] Vijay G. Anand, "*Rotating detonation combustor mechanics*," Doctor of Philosophy, Anna University, Chennai, 2018.
[43] S. Prakash and V. Raman, "The effects of mixture preburning on detonation wave propagation," in *Proceedings of the Combustion Institute*, Elsevier Ltd, pp. 3749–3758, 2021.
[44] Q. Zheng, H. L. Meng, C. S. Weng, Y. W. Wu, W. K. Feng, and M. L. Wu, "Experimental research on the instability propagation characteristics of liquid kerosene rotating detonation wave," *Defence Technology*, vol. 16, no. 6, pp. 1106–1115, 2020.
[45] S. Xu, F. Song, J. Zhou, X. Yang, and P. Cheng, "Experimental study on propagation characteristics of kerosene/air rde with different diameters," *Energies* (Basel), vol. 15, no. 12, p. 4442, 2022.
[46] S. Banagiri, P. Raj, and J. Meadows, "Numerical study of counter-rotating wave propagation in a rotating detonation engine," *Journal of Engineering for Gas Turbines and Power*, vol. 148, no. 4, p. 041017, 2026.
[47] V. Raman, S. Prakash, and M. Gamba, Nonidealities in rotating detonation engines, *Annual Review of Fluid Mechanics*, vol. 55, no. 1, pp. 639-674, 2023.
[48] J. Guo, S. Ge, Y. Guo, and J. Liang, "Experimental study on effects of different factors on continuous detonation of superfine lignite: particle size and fuel equivalent ratio," *Combustion Science and Technology*, pp. 1–25, 2024.
[49] J. Jing and H. Ma, "An experimental study on gas-solid two-phase rotating detonation ramjet engine based on aluminum powder fuel," *Journal of Physics: Conference Series*, vol. 2764, no. 1, p. 12032, 2024.
[50] X. Li, J. Li, Q. Qin, W. Jin, and L. Yuan, "Experimental study on detonation characteristics of liquid kerosene/air rotating detonation engine," *Acta Astronautica*, vol. 215, pp. 124-134, 2024.
[51] R. Driscoll, A. St. George, and E. J. Gutmark, "Numerical investigation of injection within an axisymmetric rotating detonation engine," *International Journal of Hydrogen Energy*, vol. 41, no. 3, pp. 2052–2063, 2016.